Talanta 243 (2022) 123339

Contents lists available at ScienceDirect

Talanta

journal homepage: www.elsevier.com/locate/talanta

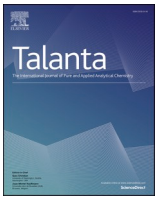

Separation of isomers using a differential mobility analyser (DMA): Comparison of experimental vs modelled ion mobility

A. Bianco [a,1,2], I. Neefjes [a,1], D. Alfaouri [a], H. Vehkamäki [a], T. Kurtén [b], L. Ahonen [a], M. Passananti [a,c,**], J. Kangasluoma [a,d,*]

[a] Institute for Atmospheric and Earth System Research/Physics, Faculty of Science, University of Helsinki, FI-00014, Finland
[b] Department of Chemistry and Institute for Atmospheric and Earth System Research (INAR), University of Helsinki, 00014, Helsinki, Finland
[c] Dipartimento di Chimica, Università di Torino, Via Pietro Giuria 5, 10125, Torino, Italy
[d] Karsa Ltd., A. I. Virtasen aukio 1, 00560 Helsinki, Finland

ARTICLE INFO

Keywords:
Mass spectrometry
Isobaric ions
Differential mobility analyser
Electrospray ionisation
Ion mobility

ABSTRACT

Mass spectrometry is uniquely suited to identify and quantify environmentally relevant molecules and molecular clusters. Mass spectrometry alone is, however, not able to distinguish between isomers. In this study, we demonstrate the use of both an experimental set-up using a differential mobility analyser, and computational ion mobility calculations for identification of isomers. In the experimental set-up, we combined electrospray ionisation with a differential mobility analyser time-of-flight mass spectrometer to separate environmentally relevant constitutional isomers, such as catechol, resorcinol and hydroquinone, and configurational isomers, such as cyclohexanediols and fatty acids (i.e., oleic and elaidic acids). Computational ion mobility predictions were obtained using the Ion Mobility Software (IMoS) program. We find that isomer separation can be achieved with the differential mobility analyser, while for catechol, resorcinol and hydroquinone, the computational predictions can reproduce the experimental order of the ion mobilities between the isomers, confirming the isomer identification. Our experimental set-up allows analysis both in the gas and liquid phase. The differential mobility analyser can, moreover, be combined with any mass spectrometry set-up, making it a versatile tool for the separation of isomers.

1. Introduction

Mass spectrometry (MS) is today a routine tool for measurements of trace compounds. It, however, only allows for the determination of the elemental composition of compounds and does not enable the separation of constitutional and configurational isomers with the same exact mass. Separation of isomers is important because they usually have different physicochemical properties and distinct biological responses. For instance, elaidic acid, the *trans* isomer of oleic acid (*cis* isomer), is connected to heart diseases. Similarly, catechol (CAT), resorcinol (RES) and hydroquinone (HYD), isomers of dihydroxybenzene, which have been widely recognised as important environmental pollutants by the US Environmental Protection Agency (EPA) and the European Union (EU), show different toxicities [1].

Isomers are separated before the mass analyser using different techniques: high performance liquid chromatography (HPLC) is commonly used for the analysis of liquid samples, while gas-chromatography (GC) is mostly used for samples in the gas phase or adsorbed on cartridges [2–6]. These techniques were widely explored in the past fifty years, and they have been often used to analyse environmental samples (e.g., natural water or air samples) in combination with sample pre-treatment and/or pre-concentration. However, one of the limitations of these techniques is that they cannot easily be used for online analysis and they are only suitable for small flow rates, generally lower than 0.3 mL min^{-1} [7]. For GC-MS and HPLC-MS, the ionisation of the analyte takes place after the chromatographic separation and several ionisation methods can be used [8,9].

In other mass spectrometric set-ups, the separation takes place after

* Corresponding author.
** Corresponding author. Institute for Atmospheric and Earth System Research/Physics, Faculty of Science, University of Helsinki, FI-00014, Finland
E-mail addresses: monica.passananti@helsinki.fi (M. Passananti), juha.kangasluoma@helsinki.fi (J. Kangasluoma).
[1] These authors contributed equally to this work.
[2] now at Laboratoire de Météorologie Physique (LaMP), CNRS/UCA, UMR 6016, Av. B. Pascal, 63,178 Aubière, France.

https://doi.org/10.1016/j.talanta.2022.123339
Received 19 November 2021; Received in revised form 24 February 2022; Accepted 26 February 2022
Available online 16 March 2022

the ionisation and, in this case, the separation is often carried out by ion-mobility separation (IMS) [10] or by differential mobility analysers (DMA) [11]. In these set-ups, the ions are generally produced using electrospray ionisation (ESI), which leads to formation of clusters composed of the neutral analyte and the reagent ion (for example NO_3^-, Cl^-, Br^-, I^-, Na^+, NH_4^+) [12]. ESI can be used for the ionisation of both gas phase and liquid phase samples. For the liquid phase analysis, the analyte is mixed with a solution containing the reagent ion and sprayed through the needle; for the analysis of analytes in the gas phase, the reagent ion is sprayed through the needle and mixed in the ESI chamber with a perpendicular flow of gas containing the analytes.

In both set-ups, ions (molecules and clusters) are separated on the basis of their mobility in a uniform electric field [11]. In particular, planar DMA has been successfully coupled to quadrupole and triple quadrupole mass spectrometry, as reported by Rus et al. [7] Compared to LC and GC separation, DMA has a shorter duty cycle (even no duty cycle when only one mobility is classified constantly), and is useable with higher flow rates, leading to potentially lower detection limits. The main difference in separation between IMS and DMA is the compromise between duty cycle and mobility resolution [13,14]. When coupled to mass spectrometers, both DMA and IMS set-ups provide simultaneously information on ion mass and on the mobility [13,15,16]. However, the DMA set-up has never been tested for isomer separation.

In recent years, computational modelling of the mobility of ions and ionic clusters has advanced rapidly. Computational mobility predictions could provide invaluable information for the identification of isomers, but the models must be validated by comparison with experiments. The programs MOBCAL [17] and Ion Mobility Software (IMoS) [18,19] provide different computational methods to calculate mobility predictions. Especially the Lennard Jones trajectory method implemented in the latter has been shown to result in near quantitative predictions [20]. To computationally predict the mobility of an ionic cluster, its minimum free energy geometry, representing the most likely configuration of the atoms in the cluster, needs to be known.

In this work, we test experimental and computational separation of different sets of isomers. The experimental set-up consists of ESI-DMA coupled to a time-of-flight (TOF) mass spectrometer with an atmospheric pressure interface (APi). As test species, we selected environmentally relevant compounds, like CAT, RES and HYD, with the molecular formula $C_6H_6O_2$. The three isomers have their two hydroxyl groups in ortho, meta and para positions, respectively, with respect to each other. They are used widely as industrial solvents impacting the aquatic and atmospheric environment. They are identified as major gas phase organic constituents, with concentrations of up to 50 ppbv, resulting from biomass burning [21], and previous studies report their toxicity for humans and the environment [22]. The molecular geometry is planar; however, the corresponding aliphatic compounds, cyclohexanediols, are not planar but present a 'chair' structure, with OH groups in either axial or equatorial positions. Cyclohexanediols can be considered as proxies of cycloterpenes, like menthol and isomenthol [23], or terpene oxidation products. We tested all possible structural isomers with molecular formula $C_6H_{12}O_2$: 1,2-cyclohexanediol, 1,3-cyclohexanediol and 1,4-cyclohexanediol. Each of these structural isomers present both *cis* and *trans* stereoisomers. To better understand the limitations of our method, we further analysed two other configurational isomers: elaidic and oleic acid. These compounds are well-known pollutants of indoor air, originating from cooking [24]. The chemical compounds of interest in this study are summarised in Table 1.

Our results show that the combination of ESI, planar DMA and APi-TOF is an effective and sensitive technique that can be used for the analysis of isomers. Identification of isomers can be tricky in absence of standards, therefore the support from computational modelling may be decisive. We compared the experimental ion mobilities of the studied analyte-charging ion clusters with mobility predictions calculated using IMoS, where the cluster minimum free energy geometries are obtained through the Jammy Key for Configurational Sampling (JKCS) program.

Table 1
Chemical compounds analysed in this study. The uncertainty reported in the column "reduced mobility" is a systematic uncertainty, always in the same direction for each class of compounds. The structural formula of configurational isomers of cyclohexanediols are reported in Table S1.

	Constitutional isomers	Geometric or configurational isomers	Mobility resolution (R) (nitrate cluster)	Reduced mobility (Z_0) (nitrate cluster)
$C_6H_6O_2$ 110.03678 g/mol	Catechol		41.9	1.76 ± 0.05 $cm^2V^{-1}s^{-1}$
	Resorcinol		42.9	1.71 ± 0.05 $cm^2V^{-1}s^{-1}$
	Hydroquinone		42.1	1.69 ± 0.05 $cm^2V^{-1}s^{-1}$
$C_6H_{12}O_2$ 116.08373 g/mol	1,2-cyclohexanediol	*Cis*-1,2-cyclohexanediol	47.2	1.64 ± 0.05 $cm^2V^{-1}s^{-1}$
		Trans-1,2-cyclohexanediol		
	1,3-cyclohexanediol	*Cis*-1,3-cyclohexanediol	48.0 and 43.1	1.68 ± 0.05 $cm^2V^{-1}s^{-1}$ and 1.63 ± 0.05 $cm^2V^{-1}s^{-1}$
		Cis-1,3-cyclohexanediol		
		Trans-1,3-cyclohexanediol		
	1,4-cyclohexanediol	*Cis*-1,4-cyclohexanediol	48.6 and 42.7	1.66 ± 0.05 $cm^2V^{-1}s^{-1}$ and 1.64 ± 0.05 $cm^2V^{-1}s^{-1}$
		Trans-1,4-cyclohexanediol		
		Trans-1,4-cyclohexanediol		
$C_{18}H_{34}O_2$ 282.25588 g/mol		Oleic acid	51.9	1.1297 ± 0.03 $cm^2V^{-1}s^{-1}$
		Elaidic acid	51.8	1.1280 ± 0.03 $cm^2V^{-1}s^{-1}$

The comparison between the experimental results and the modelled mobility allowed us to assess the accuracy of the model (IMoS) and the possibility of using IMoS to identify isomers in environmental samples.

2. Materials and methods

2.1. Chemicals

Methanol (MeOH), HYD, cyclohexanediols, elaidic acid, tetraheptylammonium bromide (THABr) (>99%) and ammonium acetate with purity grade >99% were purchased from Sigma-Aldrich, while NH_4NO_3 (>99%) was obtained from Merck and CAT and RES (>97%) from Fluka. Oleic acid food grade (65.0–88.0%) was purchased from PanReac AppliChem ITW Reagents. Stock solutions were prepared in MeOH, except the NH_4NO_3 stock solution, which was prepared in ultrapure water (MilliQ, Millipore, resistivity ~18 MΩ cm). Diluted solutions with different concentrations of analyte and NH_4NO_3 were prepared in MeOH/H_2O 80/20.

Water was sampled from the Vantaa River in Helsinki (60°23′69″ E, 24°98′74″ N) using a brown glass bottle. Filtration has been performed using a glass syringe and Millex Syringe Filter, Nylon, 0.20 μm pore size, 33 mm diameter.

2.2. Experimental set-up

The instrumental set-up is composed of an ESI-DMA source connected to the APi-TOF, as shown in detail in Figure S1. The sample line between the DMA and the APi-TOF is a 45 mm and 0.5 mm ID capillary. At the middle of the capillary there is a T split to an aerosol electrometer

to obtain the total current exiting the DMA. The inlet flow rate of the APi-TOF is 0.8 L min^{-1} and electrometer 1 L min^{-1}. The DMA was operated in counter flow mode so that ~2.5 L min^{-1} N_2 was supplied to the closed sheath flow loop, and ~0.7 L min^{-1} exited the DMA inlet. The ESI voltage is varied between −1600 and −5000 V, adapting the range to the compound signal, to obtain a current of ~60 nA at the DMA entrance; capillary flow rate is set at 16 μL min^{-1}, and kept constant for all the measurements. The silica capillary (50 μm tip i.d., 360 μm o.d., non-coated, SilicaTipTM, PicoTipTM EMITTER) was purchased from NewObjective. DMA voltage was varied using steps of 2 V of the duration of 3 s. The DMA mobility classification is calibrated before each experiment with the THABr positive monomer [25]. The APi-TOF (Tofwerk AG, Thun, Switzerland) consists of an atmospheric pressure interface (APi), made by three vacuum chambers, coupled with a time-of-flight mass spectrometer. A more detailed description of the instrument is given elsewhere [26]. The mass spectrometer mass axis is calibrated daily using HNO_3 (monomer NO_3^- and dimer $HNO_3NO_3^-$ signal) and pinonic acid.

Data was treated using the tofTools MatLab toolbox [27], as well as a newly developed in-house software, called FlatDMA-analyser. The FlatDMA-analyser allows the 2-dimensional visualisation of mass-to-charge and electrical mobility and peak-fitting of the mobility spectrum (for a more in-depth description see Supplementary S1).

2.3. Computational ion mobility modelling

Computational ion mobility predictions were obtained with the IMoS v1.10c program [19], using the Lennard Jones trajectory and projected area (PA) methods with nitrogen as carrier gas. The geometry of the lowest Gibbs free energy conformer for each analyte-charging ion dimer was obtained at the ωB97X-D/6–31++G** level of theory [28] through the JKCS configurational sampling procedure outlined by Kubečka et al. [29]. Following the JKCS procedure, the ABCluster [30], xTB [31], Gaussian 16 Rev C.01 [32], and GoodVibes [33] programs were used. Atomic partial charges were calculated with the CHelp [34], CHelpG [35], HLY [36], MK [37], Hirshfeld [38], and CM5 [39] partial charge methods at the same level of theory. For the dimers of CAT, RES, and HYD with NO_3^-, we additionally calculated the ion mobility from geometries optimised using the M06–2x [40] and PW91PW91 [41] functionals, as well as the binding free energies with electronic energy corrections at the DLPNO-CCSD(T)/aug-ccpVTZ level of theory [42]. More detailed explanations of the JKCS procedure and the ion mobility modelling methods are provided in Supplementary S2.

3. Results

3.1. Catechol, resorcinol, and hydroquinone (structural isomers)

3.1.1. Nitrate ionisation: optimisation of the experimental conditions and determination of the limit of detection and quantification

As we performed the experiments using nitrate as charging ion, we expect to observe the formation of analyte-nitrate clusters. CAT, RES and HYD have been chosen as proxies because of their planar geometry. Solutions containing 1 mM of each compound in MeOH/H_2O 80/20 have been analysed in negative mode but none of the compounds showed a distinctive signal, as would be the case for the deprotonated ion $C_6H_5O_2^-$, suggesting that the ionisation is difficult in these conditions. Nitrate or acetate have been added in the sample solution and sprayed through the ESI to produce charging ions. Different concentrations of CAT and nitrate were used to optimise the detection of the signal of the CAT-NO_3^- cluster ($C_6H_6O_2NO_3^-$), at *m/z* 172.0246 Da, and we observed that the ratio [CAT]/[NO_3^-] should not exceed the value of 1/25. The scan in the range from −1600 to −3500 V with step of 20 V and acquisition of 3 s (run duration of 4 min) allows the detection of concentration of CAT of 20 μM: this concentration is only indicative and does not represent the limit of quantification of the instrument (discussed later in this paragraph). It can be improved by decreasing the scan step or increasing the signal acquisition. For instance, performing the scan in the same interval, without varying the acquisition time but decreasing the step to 2 V (around 35 min acquisition), doubles the area of the signal of the CAT-NO_3^- cluster. Increasing the time of acquisition of the signal in the mass spectrometer increases the sensitivity of the instrument and allows the detection of compounds at low concentration. The same experiments with RES-NO_3^- showed an analogous limit of detection.

The limit of quantification (LOQ), defined as the lowest analyte concentration that can be quantitatively detected with a stated accuracy and precision for these conditions [43], was determined for a solution of CAT 40 nM, NO_3^- 1 μM. Figure S2 reports the signal as a function of the acquisition time at fixed voltage (−2550 V) and allows the determination of LOQ: a solution 40 nM needs an acquisition time longer than 300 s to have a S/N (signal to noise ratio) higher than 10 and relative error lower than 20% for a CAT-NO_3^- cluster. One of the strengths of this analytical set-up is that even low concentrations can be detected and quantified by simply increasing the acquisition time. For this reason, the acquisition of the signal for a solution CAT 4 nM, NO_3^- 1 μM shows that the signal of CAT-NO_3^- is still detectable, but it does not vary with the concentration, confirming that the sensitivity of the instrumental set-up for nitrate chemical ionisation is of the order of 4 nM (1.1 μg L^{-1}, ppb) for acquisition times of the order of 300 s, that are reasonably adapted to online analysis. Therefore, we could define the LOQ of 40 nM and the limit of detection (LOD) around 4 nM.

3.1.2. Separation of CAT, RES and HYD nitrate clusters

Three solutions containing CAT, RES and HYD 1 mM and NO_3^- 10 mM have been analysed in the same voltage interval −1600/−3500 V with scan step of 2 V. The resolution of the peak (see Supplementary S3) and the reduced mobility (Z_0; often also denoted as K_0) are reported in Table 1. Z_0 is obtained from the measured ion mobility (Z) by

$$Z_0 = \frac{P}{10,000\ Pa}\frac{273.15\ K}{T}Z, \qquad \text{Eq. 1}$$

where *P* is the pressure and *T* the temperature measured inside the DMA. It's important to note that the uncertainty on Z_0 reported in Table 1 is a systematic uncertainty, which means that it is always in the same direction for the compounds considered. The sensitivity for HYD is lower, as the signal is lower compared to the other isomers: this is due to a lower binding energy of the NO_3^- ion to the OH groups in *para* position. Computational calculations show that the binding energy of the HYD-NO_3^- cluster is around 3 kcal/mol lower than that for the CAT and RES clusters (Table S2). The mobility spectrum of the three isomers is reported in Fig. 1. We analysed a solution containing all the isomers (CAT, RES and HYD 1 mM and NO_3^- 10 mM) using the same conditions and Fig. 1 reports in black the signal intensity for the mixture solution. The peaks are partially overlapping and to identify the three peaks corresponding to CAT, RES and HYD it is necessary to deconvolute the spectrum with a peak fitting script. Using the FlatDMA-analyser software, we identified that the signal corresponds to the mass to charge ratio (*m/z*) 172.0246 Da ($C_6H_6O_2NO_3^-$). To this signal we fitted three peaks with resolution of 42 (calibrated mobility resolution of the DMA), leading to the separation of CAT, RES and HYD, with fitted peak maxima at −2490, −2563 and −2599 V, respectively (see details in Supplementary S4). The identification of the isomers is confirmed by the computational calculations, as shown later.

The same compounds can be studied as clusters with acetate but, although the separation is efficient, the stability of the clusters is lower, as described in Supplementary S5.

3.2. Cyclohexanediols

Besides the constitutional isomers CAT, RES and HYD, we also

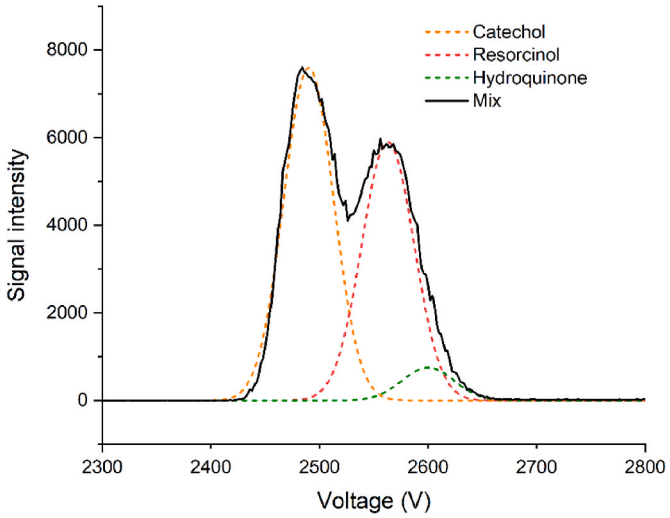

Fig. 1. Mobility spectra (with fitting and without) of catechol, resorcinol, hydroquinone, and the mixed solution.

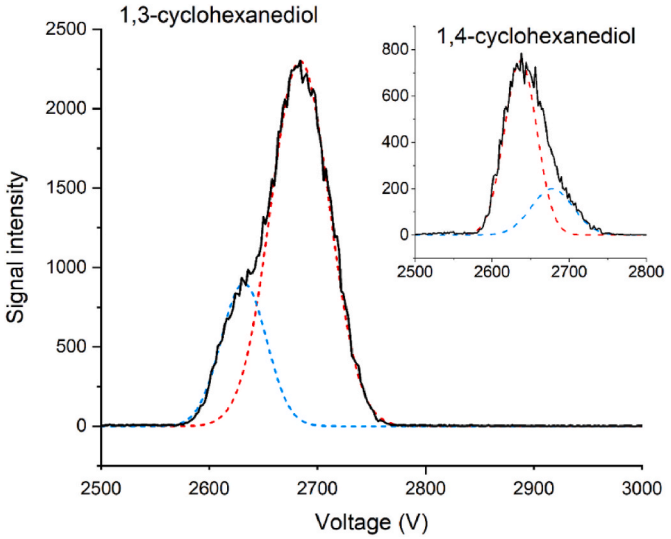

Fig. 2. Mobility spectrum for 1,3-cyclohexanediol-nitrate cluster and fit with two peaks. Inset: Mobility spectrum for 1,4-cyclohexanediol-nitrate cluster and fit with two peaks.

studied the configurational isomers 1,2-cyclohexanediol, 1,3-cyclohexanediol and 1,4-cyclohexanediol, with molecular formula $C_6H_{12}O_2$. Each of these isomers presents *cis* and *trans* stereoisomers, with the peculiarity that 1,2-cyclohexanediol presents only one *cis* and *trans* structure, while 1,3-cyclohexanediol has one *trans* and two *cis* structure and 1,4-cyclohexanediol has one *cis* and two *trans* isomers. The possible structures are collected in Table S1. For 1,2- and 1,4-cyclohexanediols, a *cis* configuration leads to one axial and one equatorial group. For *trans*-1,2-cyclohexanediol, the diaxial conformation is prevented by its high steric strain, while it may be considered for *trans*-1,4-cyclohexanediol. For 1,3-cyclohexanediol, two *cis* isomers are possible, with OH groups in equatorial and in axial configuration, respectively. The latter suffers steric interaction between the two axial groups. *Trans*-1,3-cyclohexanediol has only one isomer with axial and equatorial OH groups.

Cis and *trans* isomers of 1,2-cyclohexanediol were analysed separately. In positive mode no signal was observed.

Conformers of 1,2-cyclohexanediol (1 mM) were analysed in the presence of NO_3^- 10 mM in MeOH/H_2O 80/20. The scan in the range −1600/−3500 V with step of 2 V and acquisition of 3 s (around 35 min) shows that the NO_3^- clusters of the *cis* and *trans* isomers have the same Z_0 value within the resolution of our set-up. *Cis* and *trans* 1,2-cyclohexanediol show a similar mobility because both of the OH groups are close to each other. In this situation, the shape of the intermolecular force field around the ion is similar and produces a similar interaction between the ion and gas molecules, which leads to a similar collision cross section and mobility. 1,3-cyclohexanediol is commercially available only as a mixture of *cis* and *trans* isomers: the analysis, in the same conditions used for 1,2-cyclohexanediol, shows a peak with a clear shoulder in the mobility spectrum, at −2680 V. We fitted two peaks to the mobility spectrum, for which R and Z_0 are reported in Table 1. A similar spectrum was found for the 1,4-cyclohexanediol-nitrate cluster, which exhibits a peak at −2644 V with a shoulder at 2678 V. Peak fitting shows a good agreement for the presence of two peaks (inset in Fig. 2) and results are reported in Table 1.

The presence of two peaks can be due to the formation of nitrate clusters with different mobility for the *cis* and *trans* isomers of 1,3- and 1,4-cyclohexanediol, while the mobility is almost the same for *cis* and *trans* 1,2-cyclohexanediol because the OH groups are close in equatorial/axial and axial/axial position.

3.3. Oleic and elaidic acid

ESI-DMA-APi-TOF can resolve the signal of *cis* and *trans* conformers, as shown with the analysis of 1,3- and 1,4-cyclohexanediols, but the voltage difference is sometimes very small, depending on the location of the isomerisation. To better understand the limitations of ESI-DMA-APi-TOF set-up, two different configurational isomers with higher carbon number were tested: oleic and elaidic acid, the *cis* and *trans* isomers of $C_{18}H_{34}O_2$.

Oleic and elaidic acid (1 mM) were analysed in the presence of NO_3^- 10 mM in MeOH/H_2O 80/20. The cluster of oleic acid and nitrate has a signal at −3876 V, while the elaidic acid-nitrate cluster has a signal at −3884 V. These isomers are consequently hard to separate with the resolution of our current experimental set-up, even with the peak fitting analysis.

3.4. Experimental vs modelled mobility

Using IMoS, we calculated Z_0 values for all studied analyte-NO_3^- systems with dimer geometries obtained at the ωB97X-D/6–31++G** level of theory and partial charges obtained through the CHelp, CHelpG, MK, HLY, Hirshfeld, and CM5 partial charge methods (Table S3). For the dimers of CAT, RES, and HYD with NO_3^-, we, furthermore, calculated Z_0 values for geometries obtained with the M06–2x, and PW91PW91 functionals (Table S4). Of all partial charge methods, CHelp resulted in the lowest percentual difference to the experimental Z_0 values, with an average of 1.7% across all dimers for which the difference could be unambiguously determined (this excludes the 1,3- and 1,4-cyclohexanediols as only a mixture of *cis* and *trans* conformers were measured). The other partial charge methods, however, also performed quite well with average percentual differences of 2.0–2.1% from the experimental Z_0 values for CHelpG, MK, HLY, Hirshfeld, and CM5. Changing the ωB97X-D functional for the other two high quality DFT functionals resulted in very similar Z_0 values with no more than 0.5% difference. In the following discussion, we focus on Z_0 values with geometries obtained with the ωB97X-D functional and partial charges with the CHelp partial charge method.

Table 2 shows a comparison between the experimental Z_0 values and the modelled Z_0 values for dimers of CAT, RES, HYD with either NO_3^- or acetate as charging ions. With NO_3^- as the charging ion, the percentual difference between the experimental and modelled Z_0 values is small, ranging from −1.4 to −1.7%. The modelled ion mobilities with acetate as the charging ion are somewhat worse with differences ranging from 4.6 to 6.3%.

Despite the small difference between experiment and model for the

Table 2
The experimental reduced ion mobility (Z_0^{exp}), Lennard Jones trajectory method reduced ion mobility (Z_0^{LJTM}), percentual difference between experimental and modelled ion mobility ((Z_0^{LJTM}-Z_0^{exp})/Z_0^{exp}), and projected area ion mobility (Z^{PA}) for dimers of catechol, resorcinol, and hydroquinone with nitrate or acetate. Dimer geometries were obtained with the ωB97X-D functional and 6–31++G** basis set. Partial charges were obtained with the CHelp method.

	Z_0^{exp} ($cm^2V^{-1}s^{-1}$)	Z_0^{LJTM} ($cm^2V^{-1}s^{-1}$)	(Z_0^{LJTM}-Z_0^{exp})/Z_0^{exp} (%)	Z^{PA} ($cm^2V^{-1}s^{-1}$)
Catechol – nitrate	1.76	1.74	−1.4	2.78
Resorcinol – nitrate	1.71	1.68	−1.7	2.76
Hydroquinone – nitrate	1.69	1.66	−1.6	2.72
Catechol – acetate	1.65	1.73	4.6	2.64
Resorcinol – acetate	1.60	1.70	6.3	2.62
Hydroquinone – acetate	1.58	1.67	5.6	2.58

analyte-NO_3^- dimers, it is not possible to identify these structural isomers based on a one-to-one comparison between experimental and modelled Z_0 values. For instance, RES-NO_3^- has a modelled Z_0 value closer to the experimental Z_0 value of HYD-NO_3^- than to its own experimental Z_0 value. In other words, a quantitative analysis is not possible even with the small deviations between experiment and model, as the difference in the experimental Z_0 values between the structural isomers is likewise small.

Table 2, however, also shows that the order of the experimental Z_0 values is preserved in the modelled Z_0 values for both charging ions, with CAT having the largest Z_0 values and HYD the lowest. This is because the differences in Z_0 values between experiment and model are all in the same direction with similar magnitudes for a specific charging ion. The preservation of the experimental order indicates that the modelling approach is able to capture the geometrical differences between the isomers. Fig. 3 shows that there are indeed notable differences between the dimer geometries. CAT can form two hydrogen bonds with NO_3^- and acetate due to the position of its hydroxyl groups. RES and HYD, on the other hand, can only form one hydrogen bond with these charging ions. This difference in hydrogen bonding capacity is likely the reason for the larger difference in Z_0 value between CAT and the other two isomers. NO_3^- and acetate have virtually the same orientation with respect to the three isomers, owing to the similar position of the oxygens participating in the hydrogen bonds.

Another indication that the geometrical differences are captured by the modelling approach is that the projected area (PA) method also preserves the order of the ion mobility between the isomers, as seen in Table 2. In the PA method, the ion mobility is calculated by assuming the collision cross section is equal to the average projected area of the ion and a carrier gas molecule. This method only takes the dimer geometry into account. While the PA method results in large errors, as is typical without proper corrections, it is still able to preserve the experimental order.

The similarity in magnitude and direction of the discrepancy between model and experiment across the structural isomers points towards a systematic deviation from experiments. This systematic deviation can originate from several sources. First, the experimental ion mobilities are calibrated using the positive tetraheptylammonium ion as a calibrant. Uncertainties in the calibrant's ion mobility will systematically affect all experimental results. Similarly, differences between the temperature and pressure during the experiments and in the model set-up can result in a systematic deviation. Lastly, the Lennard Jones trajectory method is estimated to provide results some 2–4% off from experimental values [19]. This is due to various limitations, such as neglecting larger order multipoles, rotational and vibrational effects, and alignments between the carrier gas and ions. Although the influence of these limitations is generally unpredictable, it can be expected that for

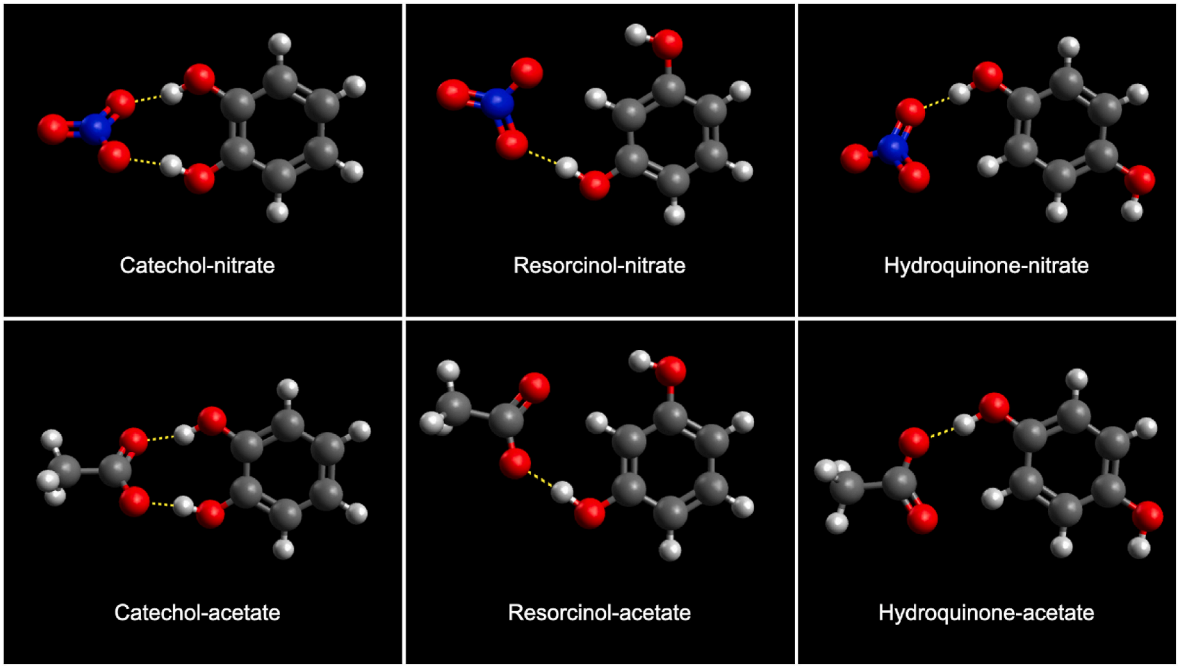

Fig. 3. The lowest Gibbs free energy conformers of dimers of catechol, resorcinol, and hydroquinone with nitrate and acetate. Geometries were obtained with the ωB97X-D functional and 6–31++G** basis set. The colour codes of the atoms are as follows: oxygen-red, nitrogen-blue, carbon-grey, hydrogen-white. Hydrogen bonds are indicated by dashed yellow lines. (For interpretation of the references to colour in this figure legend, the reader is referred to the Web version of this article.)

similar systems these limitations will have a similar effect. This is exactly what we observe. For CAT, RES, and HYD, the difference in Z_0 value between the isomers is similar in the experiments and the model, even when there is a significant absolute deviation between experiments and model.

We were able to perform a near exhaustive search for the lowest Gibbs free energy geometries of the dimers with CAT, RES, and HYD. Due to the relatively small and inflexible analyte molecules and charging ions, we could include all possible molecular conformers. We, furthermore, created enough distinct dimer conformers for a near 100% exploration of the configurational space of these small dimers [29]. While it is never certain that the global minimum Gibbs free energy structures is found, we can be quite confident that the obtained structures are close to this global minimum. This is supported by the fact that the found geometries show similar bonding with NO_3^- and acetate and provide an explanation for the larger difference in Z_0 value between CAT and the other two isomers.

We have additionally calculated the Z_0 values of the second and third lowest Gibbs free energy conformers of the dimers of CAT, RES, HYD with NO_3^- (Table S4). A change of conformer can result in a difference in Z_0 value upward of 3%. Although conformers higher in energy generally tend to have lower Z_0 values, likely due to a less compact dimer structure (Fig S7), this is by no means a systematic rule. It is, therefore, essential to find the lowest Gibbs free energy dimer structure, to avoid large unsystematic errors in the Z_0 values, possibly resulting in changes to the order between isomers.

In short, we find that the order of the experimental ion mobility is preserved in the modelled ion mobility for the CAT, RES, and HYD isomers. This characteristic is also quite robust, being consistent across the tested modelling approaches, partial charge methods, and DFT functionals. It is, however, crucial to use the correct geometry when modelling the ion mobility. In future research, it should be established if this preservation of the experimental order is present in other isomer systems. As the modelled ion mobility order is quite robust, it should also be investigated if computational methods less expensive than DFT can be used to find the geometries. If, for instance, semi-empirical methods provide a similar qualitative result, then large sets of data could be created. These large data sets could be used in a machine learning framework to study more complex systems, such as atmospheric oxidised hydrocarbons. Even if quantitative one-to-one matching is not possible, these qualitative results could help to constrain which mechanisms and yields are possible. At the same time, modelling programs, like IMoS, continuously add new functionalities that reduce their limitations, resulting in increasingly accurate ion mobility predictions [44]. If rotational and vibrational effects and alignment of the ion and carrier gas during the trajectory would be accounted for, the difference between isomers would be even better captured by the model.

Modelled Z_0 values of the cyclohexanediols and oleic and elaidic acid are presented in Table S3. For the cyclohexanediols, it is not known which experimental Z_0 value belongs to the *cis* or *trans* conformer. We can, therefore, not ascertain if the model preserves the experimental order between the isomers. At the resolution of the experimental set-up, oleic and elaidic acid were found to have the same Z_0 value (1.13 $cm^2V^{-1}s^{-1}$). The modelled Z_0 values are similarly close together, although a little higher (1.16 and 1.17 $cm^2V^{-1}s^{-1}$, respectively).

3.5. Instrument applications

The analyses presented in the previous paragraphs were performed on solutions prepared in MilliQ water. However, natural samples have a complex chemical composition, as shown, for example, for surface and atmospheric waters [45–47] which can affect the detection of compounds at low concentration, especially for mass spectrometers not working in high resolution mode. To show how DMA separation can increase the separation of isomers, surface water was sampled at the Vantaa River on September 2nd, 2020, and used to test if our method is able to separate isomers also in a complex matrix. The complete protocol is reported in Supplementary S6. River water was filtered on 0.20 μm and analysed using similar conditions to the ones described in subsection 3.1.2. For these experiments, no nitrates have been added to the solution since they are already present in sufficient concentration to achieve the ionisation. CAT, RES and HYD with final concentration of 45 μM, corresponding to 4.95 mg L^{-1}, were added to the filtered river water and analysed using ESI-DMA-APi-TOF. As shown in Figure S3, CAT, RES and HYD can be separated also at low concentration in a complex matrix like river water, with a peak resolution close to 75. This drastic resolution increment, compared to the one reported for pure standards in MilliQ water, could be correlated to the concentration of the analytes in solution but more investigation is needed to clarify this result. It's worth noting that river water has been analysed also without the addition of CAT, RES and HYD, to see if the compounds are already present in river water. We found a peak at *m/z* 172.025 Da, very close to one of the three isomers of interest at *m/z* 172.034 Da. These signals are not separated, for example, by mass spectrometers working at low resolution. However, we can exclude the presence of CAT, RES and HYD as the detected mobility does not match the mobility measured for the three compounds. This result confirms that the analysis with the set-up presented in this work can discriminate between isomers and exclude interferences by isomers with different mobility.

4. Conclusions

In this study, we used a differential mobility analyser to perform isomer separation. We achieved the separation of constitutional isomers, such as catechol, resorcinol and hydroquinone, isomers of dihydroxybenzene, as well as some configurational isomers, such as 1,3- and 1,4-cyclohexanediols. However, other configurational isomers, such as *cis* and *trans* 1,2-cyclohexanediols and 9-octadecenoic acids, cannot be separated with the resolution of our current experimental set-up. The experimental data were treated using an in-house software, FlatDMA-analyser, to consider at the same time the mobility and the mass signals and to achieve the best fit of overlapped peaks in the extracted mobility spectra. We have additionally used quantum chemical methods, combined with a configurational sampling procedure to find representative analyte–charging ion geometries, and estimated their mobility with the Ion Mobility Software (IMoS) program. For the constitutional dimers catechol, resorcinol, and hydroquinone (with the charging ions), we found that the computational ion mobility predictions were able to reproduce the order of the experimental ion mobilities between the isomers. As such, computational ion mobility predictions can assist in distinguishing between isomers.

Currently, high resolution mass spectrometers, such as the APi-TOF, are used to investigate the oxidation products of terpenes in the atmosphere, to gain insight in the oxidation mechanisms and in the formation of highly oxidised molecules that are involved in new particle formation processes. These processes lead to the formation of isomers that are impossible to separate using chemical ionisation and direct injection in the mass spectrometers. The hyphenated method presented in this study could represent a great advance in this field, since it enables the separation and detection of isomers with high sensitivity without requiring a chromatographic system. Moreover, this set-up is versatile and allows for the mobility analysis of compounds in both gas phase and liquid phase (with the SESI and ESI ionisation methods, respectively); the separation of the isomers is not affected by the complexity of the matrix, and we have demonstrated that the method can be applied to environmental samples (such as natural waters and atmospheric samples). In particular, we highlight the low LOQ reached, which can easily be improved by increasing the time of acquisition.

Credit author statement

A. Bianco: Investigation, Writing – original draft, I. Neefjes:

Investigation, Writing – original draft, D. Alfaouri: Resources, H. Vehkamäki, Funding acquisition, T. Kurtén, Funding acquisition, L. Ahonen: Software, M. Passananti: Conceptualisation, Funding acquisition, Supervision, J. Kangasluoma: Conceptualisation, Funding acquisition, Supervision. All authors reviewed and edited the draft.

Declaration of competing interest

The authors declare that they have no known competing financial interests or personal relationships that could have appeared to influence the work reported in this paper.

Acknowledgements

We thank the ERC Project 692891-DAMOCLES, Academy of Finland (project 1325656), University of Helsinki (Three-Year Research Grant 75284132) and University of Helsinki Faculty of Science ATMATH project, for funding, and the CSC-IT Center for Science in Espoo, Finland, for computational resources. We additionally thank Bernhard Reischl for stimulating discussions.

Appendix A. Supplementary data

Supplementary data to this article can be found online at https://doi.org/10.1016/j.talanta.2022.123339.

References

[1] H. Chen, J. Yao, F. Wang, Y. Zhou, K. Chen, R. Zhuang, M.M.F. Choi, G. Zaray, Toxicity of three phenolic compounds and their mixtures on the gram-positive bacteria Bacillus subtilis in the aquatic environment, Sci. Total Environ. 408 (2010) 1043–1049, https://doi.org/10.1016/j.scitotenv.2009.11.051.

[2] N. Yamamoto, T. Matsubasa, N. Kumagai, S. Mori, K. Suzuki, A diffusive badge sampler for volatile organic compounds in ambient air and determination using a thermal desorption-GC/MS system, Anal. Chem. 74 (2002) 484–487, https://doi.org/10.1021/ac010794f.

[3] C. Manzano, E. Hoh, S.L.M. Simonich, Improved separation of complex polycyclic aromatic hydrocarbon mixtures using novel column combinations in GC × GC/ToF-MS, Environ. Sci. Technol. 46 (2012) 7677–7684, https://doi.org/10.1021/es301790h.

[4] F. Hernández, M. Ibáñez, J.V. Sancho, Ó.J. Pozo, Comparison of different mass spectrometric techniques combined with liquid chromatography for confirmation of pesticides in environmental water based on the use of identification points, Anal. Chem. 76 (2004) 4349–4357, https://doi.org/10.1021/ac049768i.

[5] E. Heftmann, Chromatography: Fundamentals and Applications of Chromatography and Related Differential Migration Methods-Part B: Applications, Elsevier, 2004.

[6] E. Heftmann, Chromatography of Steroids, Elsevier, 2011.

[7] J. Rus, D. Moro, J.A. Sillero, J. Royuela, A. Casado, F. Estevez-Molinero, J.F. de la Mora, IMS–MS studies based on coupling a differential mobility analyzer (DMA) to commercial API–MS systems, Int. J. Mass Spectrom. 298 (2010) 30–40.

[8] A. Cappiello, Advances in LC-MS Instrumentation, Elsevier, 2006.

[9] E. De Hoffmann, V. Stroobant, Mass Spectrometry: Principles and Applications, John Wiley & Sons, 2007.

[10] H. Borsdorf, G.A. Eiceman, Ion mobility spectrometry: principles and applications, Appl. Spectrosc. Rev. 41 (2006) 323–375.

[11] E.O. Knutson, K.T. Whitby, Aerosol classification by electric mobility: apparatus, theory, and applications, J. Aerosol Sci. 6 (1975) 443–451, https://doi.org/10.1016/0021-8502(75)90060-9.

[12] Y. Zhao, J.K. Chan, F.D. Lopez-Hilfiker, M.A. McKeown, E.L. D'Ambro, J.G. Slowik, J.A. Riffell, J.A. Thornton, An electrospray chemical ionization source for real-time measurement of atmospheric organic and inorganic vapors, Atmos. Meas. Tech. 10 (2017) 3609–3625, https://doi.org/10.5194/amt-10-3609-2017.

[13] J.E. Krechmer, M. Groessl, X. Zhang, H. Junninen, P. Massoli, A.T. Lambe, J. R. Kimmel, M.J. Cubison, S. Graf, Y.-H. Lin, Ion mobility spectrometry–mass spectrometry (IMS–MS) for on-and offline analysis of atmospheric gas and aerosol species, Atmos. Meas. Tech. 9 (2016) 3245–3262.

[14] X. Zhang, A.T. Lambe, M.A. Upshur, W.A. Brooks, A. Gray Bé, R.J. Thomson, F. M. Geiger, J.D. Surratt, Z. Zhang, A. Gold, Highly oxygenated multifunctional compounds in α-pinene secondary organic aerosol, Environ. Sci. Technol. 51 (2017) 5932–5940.

[15] D. Oberreit, V.K. Rawat, C. Larriba-Andaluz, H. Ouyang, P.H. McMurry, C. J. Hogan Jr., Analysis of heterogeneous water vapor uptake by metal iodide cluster ions via differential mobility analysis-mass spectrometry, J. Chem. Phys. 143 (2015) 104204.

[16] C.J. Hogan Jr., J.F. De La Mora, Tandem ion mobility-mass spectrometry (IMS-MS) study of ion evaporation from ionic liquid-acetonitrile nanodrops, Phys. Chem. Chem. Phys. 11 (2009) 8079–8090.

[17] A.A. Shvartsburg, M.F. Jarrold, An exact hard-spheres scattering model for the mobilities of polyatomic ions, Chem. Phys. Lett. 261 (1996) 86–91, https://doi.org/10.1016/0009-2614(96)00941-4.

[18] C. Larriba, C.J. Hogan, Ion mobilities in diatomic gases: measurement versus prediction with non-specular scattering models, J. Phys. Chem. 117 (2013) 3887–3901, https://doi.org/10.1021/jp312432z.

[19] J. Coots, V. Gandhi, T. Onakoya, X. Chen, C. Larriba-Andaluz, A parallelized tool to calculate the electrical mobility of charged aerosol nanoparticles and ions in the gas phase, J. Aerosol Sci. 147 (2020) 105570, https://doi.org/10.1016/j.jaerosci.2020.105570.

[20] T. Wu, J. Derrick, M. Nahin, X. Chen, C. Larriba-Andaluz, Optimization of long range potential interaction parameters in ion mobility spectrometry, J. Chem. Phys. 148 (2018), 074102.

[21] P. Veres, J.M. Roberts, I.R. Burling, C. Warneke, J. de Gouw, R.J. Yokelson, Measurements of gas-phase inorganic and organic acids from biomass fires by negative-ion proton-transfer chemical-ionization mass spectrometry, J. Geophys. Res. Atmos. 115 (2010).

[22] C. Flickinger, The benzenediols: catechol, resorcinol and hydroquinone—a review of the industrial toxicology and current industrial exposure limits, Am. Ind. Hyg. Assoc. J. 37 (1976) 596–606.

[23] E.M. Davis, Advances in the enzymology of monoterpene cyclization reactions, in: Comprehensive Natural Products II, Elsevier, 2010, pp. 585–608, https://doi.org/10.1016/B978-008045382-8.00004-6.

[24] M. Takhar, C.A. Stroud, A.W.H. Chan, Volatility distribution and evaporation rates of organic aerosol from cooking oils and their evolution upon heterogeneous oxidation, ACS Earth Space Chem 3 (2019) 1717–1728, https://doi.org/10.1021/acsearthspacechem.9b00110.

[25] S. Ude, J.F. de la Mora, Molecular monodisperse mobility and mass standards from electrosprays of tetra-alkyl ammonium halides, J. Aerosol Sci. 36 (2005) 1224–1237, https://doi.org/10.1016/j.jaerosci.2005.02.009.

[26] H. Junninen, M. Ehn, T. Petäjä, L. Luosujärvi, T. Kotiaho, R. Kostiainen, U. Rohner, M. Gonin, K. Fuhrer, M. Kulmala, D.R. Worsnop, A high-resolution mass spectrometer to measure atmospheric ion composition, Atmos. Meas. Tech. 3 (2010) 1039–1053, https://doi.org/10.5194/amt-3-1039-2010.

[27] M. Passananti, E. Zapadinsky, T. Zanca, J. Kangasluoma, N. Myllys, M.P. Rissanen, T. Kurtén, M. Ehn, M. Attoui, H. Vehkamäki, How well can we predict cluster fragmentation inside a mass spectrometer? Chem. Commun. 55 (2019) 5946–5949, https://doi.org/10.1039/C9CC02896J.

[28] J.-D. Chai, M. Head-Gordon, Long-range corrected hybrid density functionals with damped atom–atom dispersion corrections, Phys. Chem. Chem. Phys. 10 (2008) 6615, https://doi.org/10.1039/b810189b.

[29] J. Kubečka, V. Besel, T. Kurtén, N. Myllys, H. Vehkamäki, Configurational sampling of noncovalent (atmospheric) molecular clusters: sulfuric acid and guanidine, J. Phys. Chem. 123 (2019) 6022–6033, https://doi.org/10.1021/acs.jpca.9b03853.

[30] J. Zhang, M. Dolg, ABCluster: the artificial bee colony algorithm for cluster global optimization, Phys. Chem. Chem. Phys. 17 (2015) 24173–24181, https://doi.org/10.1039/C5CP04060D.

[31] C. Bannwarth, S. Ehlert, S. Grimme, GFN2-xTB—an accurate and broadly parametrized self-consistent tight-binding quantum chemical method with multipole electrostatics and density-dependent dispersion contributions, J. Chem. Theor. Comput. 15 (2019) 1652–1671, https://doi.org/10.1021/acs.jctc.8b01176.

[32] M.J. Frisch, G.W. Trucks, H.B. Schlegel, G.E. Scuseria, M.A. Robb, J.R. Cheeseman, G. Scalmani, V. Barone, G.A. Petersson, H. Nakatsuji, X. Li, M. Caricato, A. V. Marenich, J. Bloino, B.G. Janesko, R. Gomperts, B. Mennucci, H.P. Hratchian, J. V. Ortiz, A.F. Izmaylov, J.L. Sonnenberg, D. Williams-Young, F. Ding, F. Lipparini, F. Egidi, J. Goings, B. Peng, A. Petrone, T. Henderson, D. Ranasinghe, V. G. Zakrzewski, J. Gao, N. Rega, G. Zheng, W. Liang, M. Hada, M. Ehara, K. Toyota, R. Fukuda, J. Hasegawa, M. Ishida, T. Nakajima, Y. Honda, O. Kitao, H. Nakai, T. Vreven, K. Throssell, J.A. Montgomery Jr., J.E. Peralta, F. Ogliaro, M. J. Bearpark, J.J. Heyd, E.N. Brothers, K.N. Kudin, V.N. Staroverov, T.A. Keith, R. Kobayashi, J. Normand, K. Raghavachari, A.P. Rendell, J.C. Burant, S.S. Iyengar, J. Tomasi, M. Cossi, J.M. Millam, M. Klene, C. Adamo, R. Cammi, J.W. Ochterski, R.L. Martin, K. Morokuma, O. Farkas, J.B. Foresman, D.J. Fox, Gaussian 16 Revision C.01, 2016.

[33] G. Luchini, J.V. Alegre-Requena, I. Funes-Ardoiz, R.S. Paton, GoodVibes: automated thermochemistry for heterogeneous computational chemistry data, F1000Res 9 (2020) 291, https://doi.org/10.12688/f1000research.22758.1.

[34] L.E. Chirlian, M.M. Francl, Atomic charges derived from electrostatic potentials: a detailed study, J. Comput. Chem. 8 (1987) 894–905, https://doi.org/10.1002/jcc.540080616.

[35] C.M. Breneman, K.B. Wiberg, Determining atom-centered monopoles from molecular electrostatic potentials. The need for high sampling density in formamide conformational analysis, J. Comput. Chem. 11 (1990) 361–373, https://doi.org/10.1002/jcc.540110311.

[36] H. Hu, Z. Lu, W. Yang, Fitting molecular electrostatic potentials from quantum mechanical calculations, J. Chem. Theor. Comput. 3 (2007) 1004–1013, https://doi.org/10.1021/ct600295n.

[37] U.C. Singh, P.A. Kollman, An approach to computing electrostatic charges for molecules, J. Comput. Chem. 5 (1984) 129–145, https://doi.org/10.1002/jcc.540050204.

[38] F.L. Hirshfeld, Bonded-atom fragments for describing molecular charge densities, Theor. Chim. Acta 44 (1977) 129–138, https://doi.org/10.1007/BF00549096.

[39] A.V. Marenich, S.V. Jerome, C.J. Cramer, D.G. Truhlar, Charge model 5: an extension of Hirshfeld population analysis for the accurate description of molecular interactions in gaseous and condensed phases, J. Chem. Theor. Comput. 8 (2012) 527–541, https://doi.org/10.1021/ct200866d.

[40] Y. Zhao, D.G. Truhlar, The M06 suite of density functionals for main group thermochemistry, thermochemical kinetics, noncovalent interactions, excited states, and transition elements: two new functionals and systematic testing of four M06-class functionals and 12 other functionals, Theor Chem Account 120 (2008) 215–241, https://doi.org/10.1007/s00214-007-0310-x.

[41] J.P. Perdew, Y. Wang, Accurate and simple analytic representation of the electron-gas correlation energy, Phys. Rev. B 45 (1992) 13244–13249, https://doi.org/10.1103/PhysRevB.45.13244.

[42] C. Riplinger, F. Neese, An efficient and near linear scaling pair natural orbital based local coupled cluster method, J. Chem. Phys. 138 (2013), 034106, https://doi.org/10.1063/1.4773581.

[43] D.A. Armbruster, T. Pry, Limit of blank, limit of detection and limit of quantitation, Clin. Biochem. Rev. 29 (Suppl 1) (2008). S49–S52.

[44] C. Larriba-Andaluz, J.S. Prell, Fundamentals of ion mobility in the free molecular regime. Interlacing the past, present and future of ion mobility calculations, Int. Rev. Phys. Chem. 39 (2020) 569–623, https://doi.org/10.1080/0144235X.2020.1826708.

[45] A. Bianco, L. Deguillaume, M. Vaïtilingom, E. Nicol, J.-L. Baray, N. Chaumerliac, M.C. Bridoux, Molecular Characterization of Cloud Water Samples Collected at the puy de Dôme (France) by Fourier Transform Ion Cyclotron Resonance Mass Spectrometry, Environmental Science & Technology, 2018, https://doi.org/10.1021/acs.est.8b01964.

[46] M.-H. Lee, Y.K. Lee, M. Derrien, K. Choi, K.H. Shin, K.-S. Jang, J. Hur, Evaluating the contributions of different organic matter sources to urban river water during a storm event via optical indices and molecular composition, Water Res. 165 (2019) 115006, https://doi.org/10.1016/j.watres.2019.115006.

[47] Y. Lu, X. Li, R. Mesfioui, J.E. Bauer, R.M. Chambers, E.A. Canuel, P.G. Hatcher, Use of ESI-FTICR-MS to characterize dissolved organic matter in headwater streams draining forest-dominated and pasture-dominated watersheds, PLoS One 10 (2015), e0145639, https://doi.org/10.1371/journal.pone.0145639.